International Journal of Mechanical Sciences 115-116 (2016) 360–369

Contents lists available at ScienceDirect

International Journal of Mechanical Sciences

journal homepage: www.elsevier.com/locate/ijmecsci

Coupled hydrogen diffusion simulation using a heat transfer analogy

A. Díaz *, J.M. Alegre, I.I. Cuesta

Structural Integrity Group, Escuela Politécnica Superior, Avda. Cantabria s/n, 09006 Burgos, Spain

ARTICLE INFO

Article history:
Received 10 June 2016
Received in revised form
8 July 2016
Accepted 18 July 2016
Available online 19 July 2016

Keywords:
Hydrogen diffusion
Finite elements
Fracture mechanics
Elasto-plastic coupling

ABSTRACT

Simulations of Hydrogen Assisted Cracking (HAC) in metals and alloys include hydrogen concentration as a crucial variable. With this objective, phenomenological diffusion models that consider chemical potential gradients as the driving force for diffusion are described. Equations are then modified to include the influence of the stress-strain state and trapping.

A crack tip, whose field of stresses and displacements is described by fracture mechanics, is modelled while diffusion equations are implemented through subroutines in the commercial program ABAQUS by means of the analogy between diffusion equations and heat transfer. Effects of trapping on hydrogen transport are then discussed. Moreover, hydrogen induces a lattice dilatation and a modification of the local plastic flow; this coupled behaviour is also modelled through the heat transfer analogy. Finally, stress-dependent boundary conditions are implemented, representing hydrogen entry in a more realistic way.

1. Introduction

Metals and alloys are degraded in the presence of hydrogen. One of these phenomena is known as hydrogen embrittlement, and mechanisms that operate at the microscopic and atomic levels are still not entirely clear. Modelling the interaction between hydrogen and the material in a crack tip is essential, because hydrogen drastically affects fracture behaviour. So damage models, both continuous damage models and cohesive models, must incorporate a new variable: hydrogen concentration. This paper aims to contribute to this first step in the hydrogen embrittlement modelling, i.e. to predict accurate hydrogen distributions near a crack tip.

With this objective, diffusion equations are derived from Fick's laws which describe the hydrogen flux due to a concentration gradient. Trapping is considered within this model in an explicit form in such a way that diffusion variables (concentration, occupancy, chemical potential and flux) are distinguished depending on whether hydrogen is in a lattice or a trapping site. These equations are also modified by the stress-strain field.

In order to properly include hydrogen trapping, there is currently no commercial Finite Element software in which these equations are implemented by default. It has been necessary, therefore, to develop a subroutine based on the analogy between diffusion and heat transfer. This procedure has been verified by simulating hydrogen diffusion near a crack tip with a boundary layer approach, using the same geometry and parameters as those first proposed by Sofronis and McMeeking [1] for hydrogen in iron. This simulation has been repeatedly revisited in literature for the sake of comparison, and some improvements have been made: the inclusion of a plastic strain rate [2], the consideration of coupled diffusion [3,4] and stress-state dependent boundary conditions [5]. All of these improvements are discussed in the present paper and are implemented in Finite Element simulations following the analogy between diffusion and heat transfer. Emphasis is also put on the range of validity of the simplification usually assumed in diffusion models.

2. Hydrogen diffusion phenomenological model

Hydrogen Assisted Cracking must be modelled in a continuous scale in order to handle the stress-strain fields. For this reason, diffusion equations describing hydrogen transport are usually based on a phenomenological approach in which vector fluxes and mass balances are defined over the material domain [6].

Hydrogen atoms promote decohesion, modify dislocation motion and alter material properties in many different ways. In addition, the stress-strain field influences hydrogen transport by means of two phenomena: hydrostatic stress, which produces lattice dilatation so hydrogen will tend to reach expanded sites, and plastic strain, which increases the amount of crystal defects creating trapping sites.

* Corresponding author.
E-mail address: adportugal@ubu.es (A. Díaz).

http://dx.doi.org/10.1016/j.ijmecsci.2016.07.020
0020-7403/

The latter phenomenon is crucial in a crack tip where plastic strain is highly localized. This is why hydrogen diffusion models consider a two-level approach as if there were two different chemical components. That is to say hydrogen might be localized in lattice sites (L subscript) or trapping sites (T subscript).

2.1. Fluxes

As it was noted, hydrogen diffusion models in metals usually consider two types of sites. Within the framework of non-equilibrium thermodynamics, mass fluxes derived from Onsager relationships are taken into account [7,8]. Even though mass concentration is the sought variable, chemical potential gradients $\nabla\mu_j$ represent the thermodynamic driving force which produces diffusion. Onsager coefficients L_{ij} denote the action of force j on component i; negative sign indicates that the net movement of i-type hydrogen atoms, i.e. hydrogen flux J_i, occurs from high to low chemical potential regions:

$$J_i = -\sum_{j=1}^{n} L_{ij}\nabla\mu_j \tag{1}$$

Particularly, for the two-level diffusion model accounting for lattice and trapping sites, fluxes might be expressed in a matrix form:

$$\begin{bmatrix} J_L \\ J_T \end{bmatrix} = \begin{bmatrix} L_{LL} & L_{LT} \\ L_{TL} & L_{TT} \end{bmatrix} \begin{bmatrix} \nabla\mu_L \\ \nabla\mu_T \end{bmatrix} \tag{2}$$

However, it is usually assumed that the gradient of μ_L does not affect the flux between trapping sites and the gradient of μ_T does not affect the flux between lattice sites. Cross-terms are thus neglected, L_{LT}=L_{TL}=0, so:

$$J_L = -L_{LL}\nabla\mu_L \tag{3}$$

$$J_T = -L_{TT}\nabla\mu_T \tag{4}$$

Onsager coefficients are related to the Einstein equation of diffusion,

$$L_{LL} = \frac{D_{LL}}{RT}C_L \tag{5}$$

$$L_{TT} = \frac{D_{TT}}{RT}C_T \tag{6}$$

where D_{LL} is the lattice diffusivity, D_{TT} is the diffusivity between trapping sites, C_L and C_T are the hydrogen concentrations in lattice and trapping sites respectively, R is the universal constant of gases and T is the absolute temperature.

Additionally, chemical potential can be expressed in terms of hydrogen concentration. More precisely, it is related to occupancy of i-sites θ_i=C_i/N_i, where N_i is the concentration of i-sites. From interstitial solid solutions thermodynamic theory, chemical potential usually comprises a term depending on configurational entropy, thus on occupancy, and another term μ_i^0 which express the chemical potential in the standard state. Influence of stress state is considered by means of a purely dilatational term, therefore a term is added consisting of hydrostatic stress σ_h=$\frac{1}{3}trace(\sigma)$ multiplied by the partial molar volume of hydrogen inside the metal $\bar{V}_H$. In the present work, it has been assumed, as it was by Di Leo et al. [5], that the chemical expansion is the same for lattice sites and trapping sites:

$$\mu_L = \mu_L^0 + RT\ \ln\frac{\theta_L}{1-\theta_L} - \bar{V}_H\sigma_h \tag{7}$$

$$\mu_T = \mu_T^0 + RT\ \ln\frac{\theta_T}{1-\theta_T} - \bar{V}_H\sigma_h \tag{8}$$

Substituting (5)–(8) into (3)–(4) gives:

$$J_L = -D_{LL}\frac{C_L}{(1-\theta_L)}\left(\frac{\nabla C_L}{C_L} - \frac{\nabla N_L}{N_L}\right) + \frac{D_{LL}}{RT}C_L\bar{V}_H\nabla\sigma_h \tag{9}$$

$$J_T = -D_{TT}\frac{C_T}{(1-\theta_T)}\left(\frac{\nabla C_T}{C_T} - \frac{\nabla N_T}{N_T}\right) + \frac{D_{TT}}{RT}C_T\bar{V}_H\nabla\sigma_h \tag{10}$$

2.2. Mass balance

In order to relate fluxes, which are established due to the chemical potential gradient, with concentration variation, a mass balance is required. Assuming no internal sources of hydrogen, the variation of total hydrogen concentration in a volume V must be equal to the flux through the surrounding surface S of such a volume:

$$\frac{d}{dt}\int_V (C_L + C_T)dV = -\int_S (J_L + J_T)\cdot n dS \tag{11}$$

Surface is orientated outwards, so negative sign means that positive fluxes represent hydrogen exit from the volume.

2.3. Simplified model

These expressions are usually simplified considering the following facts:

- Interstitial sites concentration is assumed constant: ∇N_L=0. This is arguably because as traps are created the number of interstitial sites could be modified.
- In many alloys, especially in bcc lattices, it is expected low occupancy $\theta_L \ll 1$ because $N_L \gg C_L$. However, θ_L may not be small in FCC metals [9].
- Mobility between trapping sites, or equivalently diffusion coefficient, is considered near zero: $D_{TT}\approx 0$, because traps are not connected or because their deep potential energy well prevents hydrogen from diffusing, i.e. $\Delta E_{TT} \gg 1$. This will be discussed in detail in Section 5.

Assuming these simulifications, fluxes might be expressed as follows:

$$J_L = -D_{LL}\nabla C_L + \frac{D_{LL}}{RT}C_L\bar{V}_H\nabla\sigma_h \tag{12}$$

$$J_T = 0 \tag{13}$$

According to divergence theorem, Eq. (11) can be expressed:

$$\int_V \frac{d}{dt}(C_L + C_T)dV = -\int_V \nabla\cdot J_L\, dV \tag{14}$$

The balance equation to be solved is then:

$$\frac{dC_L}{dt} + \frac{dC_T}{dt} + \nabla\cdot J_L = 0 \tag{15}$$

2.4. Equilibrium

Having two unknowns (C_L and C_T), both variables should connected using kinetic or thermodynamic assumptions. In this paper, equilibrium between the traps and interstitial sites is considered, i.e. μ_L=μ_T, which leads to the so-called Oriani's equilibrium [10]:

$$\frac{\theta_T}{1-\theta_T} = \frac{\theta_L}{1-\theta_L} K_T \tag{16}$$

Where $K_T = \exp\left(-\frac{E_b}{RT}\right)$ and the binding energy, inherently negative [1], is defined as the difference $\mu_L^0 - \mu_T^0$. When thermodynamic equilibrium cannot be assumed, McNabb and Foster [11] formulation must be included in diffusion equations. Operating in (16) with the assumption that $\theta_L \ll 1$, C_T might be expressed in terms of lattice concentration C_L:

$$C_T = \frac{N_T}{1 + \frac{N_L}{C_L K_T}} \tag{17}$$

2.5. Plastic strain influence

Concentration of trapping sites N_T has been has been demonstrated dependent on plastic strain. Variations of C_T with time must account for the rate at which traps are created. Thus applying the chain rule [2]:

$$\frac{dC_T}{dt} = \frac{dC_T}{dC_L}\frac{dC_L}{dt} + \frac{dC_T}{dN_T}\frac{dN_T}{d\varepsilon^p}\frac{d\varepsilon^p}{dt} \tag{18}$$

Where ε^p is the equivalent plastic strain, defined by means of the plastic part of the deformation rate tensor $\mathbf{D}_{ij}^p$:

$$\varepsilon^p = \int_0^t \sqrt{\frac{2}{3}\mathbf{D}_{ij}^p \mathbf{D}_{ij}^p}\, dt \tag{19}$$

And including the derivatives from Eq. (17) and $dC_T/dN_T = \theta_T$:

$$\frac{dC_T}{dt} = \frac{C_T(1-\theta_T)}{C_L}\frac{dC_L}{dt} + \theta_T \frac{dN_T}{d\varepsilon^p}\frac{d\varepsilon^p}{dt} \tag{20}$$

Number of trapping sites increases with plastic strain as crystal defects are created; a theoretical expression is hard to find so the expression $N_T = N_T(\varepsilon^p)$ usually is fitted by means of electrochemical permeation test. For bcc iron, it is sometimes used the relationship obtained by Kumnick and Johnson [12]:

$$\log N_T = 23.26 - 2.33 \exp(-5.5\varepsilon^p) \tag{21}$$

Diffusion model proposed by Sofronis and McMeeking [1] with the plastic strain rate term introduced by Krom et al. [2] is finally attained:

$$\left(\frac{C_T(1-\theta_T)}{C_L} + 1\right)\frac{\partial C_L}{\partial t} + \theta_T \frac{dN_T}{d\varepsilon^p}\frac{d\varepsilon^p}{dt} - \nabla\cdot\left(D_L \nabla C_L\right) + \nabla\cdot\left(\frac{D_L C_L \bar{V}_H}{RT}\nabla\sigma_h\right) = 0 \tag{22}$$

An effective diffusion coefficient might be defined:

$$\frac{D_L}{D_{eff}}\frac{\partial C_L}{\partial t} + \theta_T \frac{dN_T}{d\varepsilon^p}\frac{d\varepsilon^p}{dt} - \nabla\cdot\left(D_L \nabla C_L\right) + \nabla\cdot\left(\frac{D_L C_L \bar{V}_H}{RT}\nabla\sigma_h\right) = 0 \tag{23}$$

3. Coupled diffusion

Transport equations include stress-strain variables; hydrostatic stress and equivalent plastic strain is this case. Similarly, constitutive elasto-plastic equations which model material behaviour might be influenced by *internal variables*, e.g. hydrogen concentration. Two phenomena are usually included in this coupled response: hydrogen induced dilatation and hydrogen induced softening.

3.1. Hydrogen induced dilatation

If only a pure dilatational distortion of the metal lattice is considered, a volumetric strain is introduced [4]:

$$e_{vol}^t = (c - c_0)\frac{\Delta v}{\Omega} \tag{24}$$

With c and c_0, local and initial concentrations respectively (measured in H atoms per metal atom); and where, Δv is the volume change for each introduced hydrogen atom and Ω is the mean volume of a metal atom.

A term $\mathbf{D}_{ij}^h$ including this expansion is added to the plastic and elastic terms in the total deformation rate tensor. Volumetric engineering strain is translated into true linear strain and a parameter $\lambda = \Delta v/\Omega$ is inserted:

$$\mathbf{D}_{ij}^h = \frac{d}{dt}\left[\ln\left(1 + \frac{\lambda(c-c_0)}{3}\right)\right]\delta_{ij} \tag{25}$$

Considering every variable constant respect to time, except concentration c, dilatational rate tensor takes the form:

$$\mathbf{D}_{ij}^h = \frac{\lambda}{3 + \lambda(c-c_0)}\frac{dc}{dt}\delta_{ij} \tag{26}$$

3.2. Hydrogen induced softening

Embrittlement promoted by hydrogen could lead to think in a local hardening but, experimentally, Birnbaum and Sofronis [13] demonstrated that hydrogen enhances dislocation motion causing a local softening. Nonetheless, hydrogen may increase or decrease flow stress at the macroscale. Mechanisms by which there is sometimes local softening while macroscopically hydrogen causes shear localization are not yet understood [3].

Following Sofronis' works, local flow stress is modelled as a function of total concentration c Here, the factor ξ is taken following Kotake et al. [14]. Last multiplying term represents a hardening exponential function where σ_0 is the initial yield stress, E is the Young modulus, ε^p the equivalent plastic strain and n the hardening exponent.

$$\sigma_{ys}(\varepsilon^p, c) = (\xi c + 1)\sigma_0\left(1 + \frac{E}{\sigma_0}\varepsilon^p\right)^n \tag{27}$$

Depending on the specific conditions, ξ might be a softening parameter ($\xi<0$) or a hardening parameter ($\xi>0$). An experimental fitting is recommended due to the lack of physical base of this parameter.

4. Heat transfer analogy

Due to the scarce versatility allowed by mass diffusion analysis in Finite Element commercial codes, some authors have used the analogy comparing heat transfer and diffusion for numerical implementation [15–17].

Transport phenomena are described by similar balance equations and fluxes. Particularly, momentum exchange is studied in viscous fluids, energy exchange in heat transfer analysis and mass exchange in diffusion processes [18]. This work puts the focus on the analogy between the last two phenomena. ABAQUS is the commercial software used, so different subroutines are written in order to modify the thermal analysis and obtain concentration distributions in Finite Element simulations. Barrera et al. [19] have recently discussed the numerical details for the implementation of this thermal analogy, improving the numerical procedure previously proposed by Oh et al. [15]. Regarding diffusion equations, a

consistent approach with [19] is followed in the next section although here the coupling effects and the boundary conditions are modelled in a different way.

4.1. Diffusion equations

The energy balance for a solid stationary [18] is analogous to Eq. (11). ABAQUS consider the balance in the following form:

$$\int_V \rho \frac{d\hat{U}}{dt} dV = \int_S q dS + \int_V r dV \tag{28}$$

$$\rho \frac{d\hat{U}}{dt} + \nabla \cdot q = 0 \tag{29}$$

Heat flux $\vec{q}$ depends on the temperature gradient according to Fourier's law. And $\hat{U}$ is the internal energy per unit mass. If we set the density equal to one, total hydrogen concentration might be regarded as the internal energy per unit mass. Both are the conserved quantities in the global balance. This fact was already noted by Barrera et al. [19]: the analogous variable to the internal energy $\hat{U}$ is total concentration C, and not the chemical potential as was suggested by Oh et al. [15].

At constant pressure, a relationship between the variation of that energy and temperature can be defined as specific heat capacity c_P:

$$d\hat{U} = c_P dT \tag{30}$$

Analogically the term D_{eff}/D_L relates dC with dC_L, but in this case the plastic strain rate term has also been included. Because both factors depend on hydrogen concentrations, a UMATHT subroutine is used. Diffusivity in Fick's first law correspond to conductivity in Fourier's law, but this is not important since fluxes are completely redefined following Eqs. (12) and (13). Table 1 summarizes analogies between variables.

Within the UMATHT interface, it is not necessary to explicitly calculate the gradient ∇C_L as its analogous variable DTEMDX is already available. However, as shown in Section 2, hydrogen flux always depends on the hydrostatic stress gradient. The user subroutine USDFLD allows to access the value of the hydrostatic stress at the integration points of an element $[\sigma_h]_{el}$. Then, the 2D gradient of hydrostatic stress at any point $\left[\nabla\sigma_h\right]_{x,y}$ is obtained by means of the gradient matrix $\left[\mathbf{B}\right]$:

$$\left[\nabla\sigma_h\right]_{x,y} = \left[\mathbf{B}\right]\cdot[\sigma_h]_{el} \tag{31}$$

In the performed simulations elements with four integration points have been used, so there are four values in the vector $[\sigma_h]_{el}$ and four shape functions N_i. Thus, Eq. (31) might be rewritten as:

$$\begin{bmatrix} \frac{\partial\sigma_h}{\partial x} \\ \frac{\partial\sigma_h}{\partial y} \end{bmatrix}_{x,y} = \begin{bmatrix} \frac{\partial N_1}{\partial x} & \frac{\partial N_2}{\partial x} & \frac{\partial N_3}{\partial x} & \frac{\partial N_4}{\partial x} \\ \frac{\partial N_1}{\partial y} & \frac{\partial N_2}{\partial y} & \frac{\partial N_3}{\partial y} & \frac{\partial N_4}{\partial y} \end{bmatrix} \begin{bmatrix} \sigma_{h,1} \\ \sigma_{h,2} \\ \sigma_{h,3} \\ \sigma_{h,4} \end{bmatrix}_{el} \tag{32}$$

Table 1
Analogy between variables in heat transfer and diffusion.

Heat transfer	Diffusion
Internal energy per unit mass: $\hat{U}$	Total concentration: C
Heat flux: $\vec{q}$	Mass flux: $\vec{J}$
Temperature: T	Concentration in lattice sites: C_L
Specific heat capacity: c_p	D_L/D_{eff}
Density: ρ	1

In order to obtain the derivatives of the shape functions included in $\left[\mathbf{B}\right]$, the inverse of the Jacobian matrix $[\mathbf{J}]^{-1}$, must be used.

$$\begin{bmatrix} \frac{\partial N_i}{\partial x} \\ \frac{\partial N_i}{\partial y} \end{bmatrix} = [\mathbf{J}]^{-1} \begin{bmatrix} \frac{\partial N_i}{\partial \xi} \\ \frac{\partial N_i}{\partial \eta} \end{bmatrix} \tag{33}$$

This Jacobian matrix corresponds to the transformation from global to natural coordinates, i.e. the mapping from the global system (x, y) to the isoparametric system (ξ, η):

$$[\mathbf{J}] = \begin{bmatrix} \frac{\partial x}{\partial \xi} & \frac{\partial y}{\partial \xi} \\ \frac{\partial x}{\partial \eta} & \frac{\partial y}{\partial \eta} \end{bmatrix} = \begin{bmatrix} \sum_{i=1}^{4} \frac{\partial N_i}{\partial \xi} x_i & \sum_{i=1}^{4} \frac{\partial N_i}{\partial \xi} y_i \\ \sum_{i=1}^{4} \frac{\partial N_i}{\partial \eta} x_i & \sum_{i=1}^{4} \frac{\partial N_i}{\partial \eta} y_i \end{bmatrix} \tag{34}$$

In Section 5, the determination of ∇C_T and $\nabla \varepsilon_p$ is also required so a similar procedure is followed there, once the values at integration points are known.

4.2. Coupling equations

Coupled effects on hydrogen diffusion explained on Section 3 are usually inserted by means of a UMAT in ABAQUS. Here, for the sake of simplicity, the analogy with heat transfer is exploited again. The advantage is that constitutive elasto-plastic equations have not to be modified and tangent stiffness matrix has not to be recalculated as it is in other works [14,20]. In an incremental form, deformation rate term due to hydrogen dilatation can be expressed:

$$\Delta\varepsilon_{ij}^{h} = \frac{\lambda}{3 + \lambda(c - c_0)} \Delta c \delta_{ij} \tag{35}$$

This reminds a thermal expansion strain considered purely dilatational which is introduced in ABAQUS by means of UEXPAN subroutine.

$$\Delta\varepsilon_{ij}^{T} = \alpha(T)\Delta T\delta_{ij} \tag{36}$$

Therefore a coefficient alpha is redefined as:

$$\alpha(c) = \frac{\lambda}{3 + \lambda(c - c_0)} \tag{37}$$

On the other hand, local softening is modelled taking advantage of UHARD subroutine where yield stress may be redefined by the user as a function of plastic strain and temperature, in this case plastic strain and concentration (Fig. 1).

4.3. Validation of diffusion models

Diffusion near a crack tip is simulated following the pioneering work of Sofronis and McMeeking [1]. In order to validate the heat transfer subroutine, the following scenarios are considered:

- Diffusion general equation without plastic strain rate. Results are then compared with those of Sofronis and McMeeking [1].
- Diffusion general equation with plastic strain rate. Results are then compared with those of Krom et al. [2].

4.3.1. Parameters

The simulated material is bcc iron as it is was chosen by Sofronis and McMeeking in its pioneer work and afterwards reproduced by many authors. Therefore, all simulation parameters are obtained from such Ref. [1].

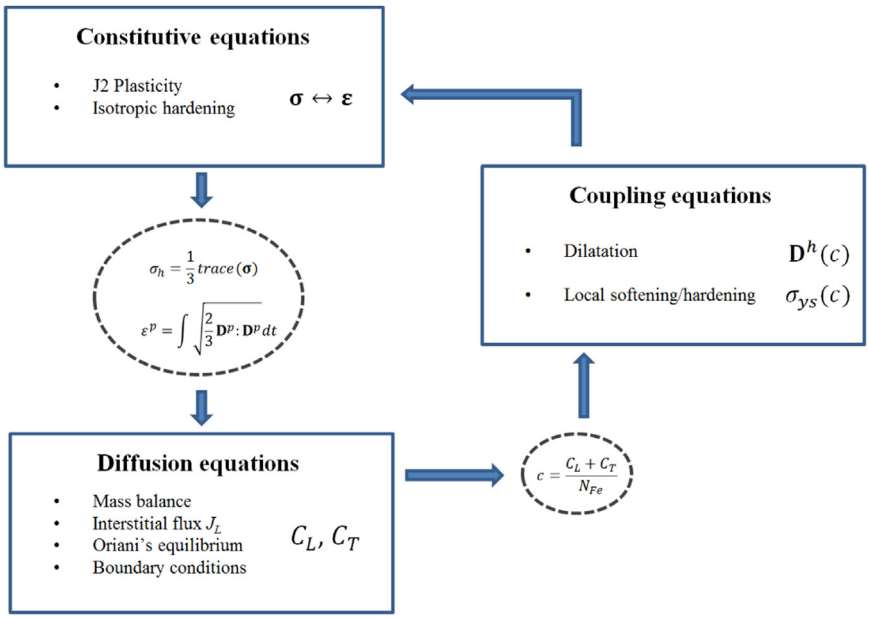

Fig. 1. Coupling scheme between diffusion and elasto-plastic response.

It is worth mentioning that N_L has been obtained assuming the usual density and atomic weight of iron (ρ_{Fe}=7. 87 g/cm^3, A_{Fe}=55. 845 g/mol) and a parameter β=6 which means that, in a bcc lattice, there are six interstitial sites for each iron atom.

$$N_L = \beta N_{Fe} = \beta \frac{\rho_{Fe} \cdot N_A}{A_{Fe}} \tag{38}$$

Binding energy of −60 kJ/mol represents an irreversible trap if the limit proposed by [10] is taken into account. However, this limit depends on kinetics of diffusion and on temperature in particular.

Classical J2 plasticity and isotropic hardening is considered. Elasto-plastic material behaviour is modelled by a power law [2], being the relationship between uniaxial stresses and strains $\sigma - \varepsilon$:

$$\varepsilon = \begin{cases} \dfrac{\sigma}{E} & \text{si } \varepsilon \le \dfrac{\sigma_{ys}}{E} \\ \dfrac{\sigma_{ys}}{E}\left(\dfrac{\sigma}{\sigma_{ys}}\right)^n & \text{si } \varepsilon > \dfrac{\sigma_{ys}}{E} \end{cases} \tag{39}$$

where E is the Young's modulus, σ_{ys} the yield strength and n the hardening coefficient. Table 2 shows the material parameters both mechanical (left column) and related to diffusion (right column).

The expression N_T=$N_T(\varepsilon^p)$ is fitted from the permeation tests performed by Kumnick and Johnson [12] above mentioned, with N_T in units of number of traps per cubic meter.

Environmental parameters are: a temperature of 300 K and the hydrogen concentration in the boundary highlighted in Fig. 2 which is equal to an equilibrium concentration C_{eq}=2. 08·10^{12} H atoms/mm^3 [1]; this is a very low concentration, as it is expected in an iron-hydrogen system, corresponding in weight parts per million to C_{eq}=4. 424·10^{-4} wppm.

Table 2
Elasto-plastic (left) and diffusion (right) parameters (from Ref. [1]).

E	207,000 MPa	D_L	$1.27 \cdot 10^{-2}$ mm^2/s
ν	0.3	N_L	$5.1 \cdot 10^{20}$ sites/mm^{-3}
σ_{ys}	250 MPa	$\bar{V}_H$	2000 mm^3/mol
n	5	E_b	−60 kJ/mol

4.3.2. Geometry and boundary conditions

Plane strain conditions in which the plastic zone is confined (yielding small scale) are simulated. Therefore Liner Elastic Fracture Mechanics are applied. With the aim of reproducing the stress state in a crack tip, the finite model is replaced by an "infinite" material and a "semi-infinite"crack; correspondent displacements (in a remote radius) are imposed as boundary conditions. This is the so-called "boundary layer approach". Plane strain conditions lead to the following displacements u_x in x direction and u_y in y direction:

$$\begin{cases} u_x(R,\theta) = K_I \dfrac{1+\nu}{E}\sqrt{\dfrac{R}{2\pi}}\ \cos\left(\dfrac{\theta}{2}\right)\left[2 - 4\nu + 2\sin^2\left(\dfrac{\theta}{2}\right)\right] \\ u_y(R,\theta) = K_I \dfrac{1+\nu}{E}\sqrt{\dfrac{R}{2\pi}}\ \sin\left(\dfrac{\theta}{2}\right)\left[4 - 4\nu + 2\cos^2\left(\dfrac{\theta}{2}\right)\right] \end{cases} \tag{40}$$

where the outer radius is R=0. 15 m and θ is the angle in radians from the crack plane of crack (Fig. 2). Load, and therefore the stress state, increases from 0 to its maximum value K_I=89.2 MPa$\sqrt{\text{m}}$ during the first 130 s of simulation. Thereafter, it remains constant until 1419 h.

Initial crack tip radius is equal to the half of initial crack opening $b_0/2$ = 0. 01 mm (Fig. 2). As $R \gg b_0/2$, remoteness of applied displacements is ensured.

Regarding the mesh, it has been refined in this work respect original Refs. [1,2,5] in order to better capture all phenomena occurring in the crack tip. To do this, geometry is divided in two parts: until 0.05 mm from the crack tip, the side of the elements is a regular dimension (about 0.0025 mm), from there that dimension grows radially by a factor of 1.29 (Fig. 2). This procedure results in a total of 4073 nodes and 1308 elements CPE8RT type (quadrilateral elements for plane strain, 8 nodes with reduced formulation and used for heat transfer).

Besides imposed displacements, symmetry must be considered as another boundary condition restricting the movement perpendicular to the plane of symmetry (Fig. 2). A boundary concentration equal to equilibrium hydrogen lattice concentration C_b=C_{eq} is also imposed in the crack face (right picture in Fig. 2 in blue).

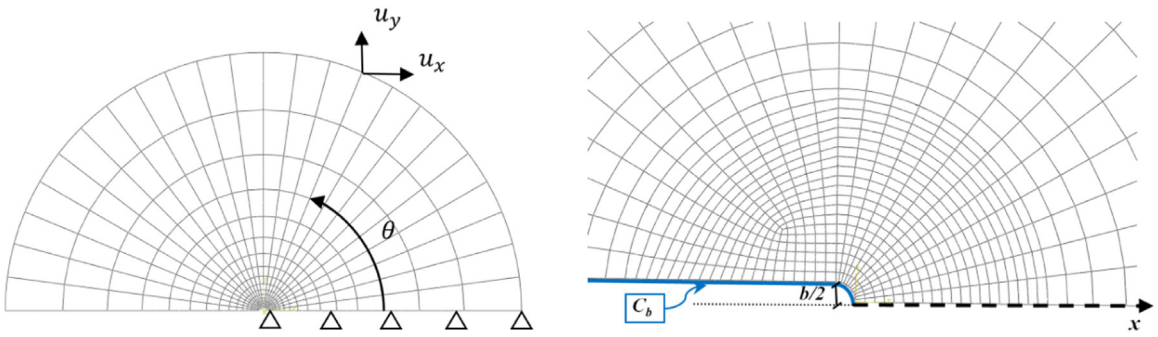

Fig. 2. Boundary layer geometry (left). Mesh detail in a crack tip with initial radios of $b_0/2$ and hydrogen concentration C_b in the boundary (right). (For interpretation of the references to color in this figure, the reader is referred to the web version of this article.)

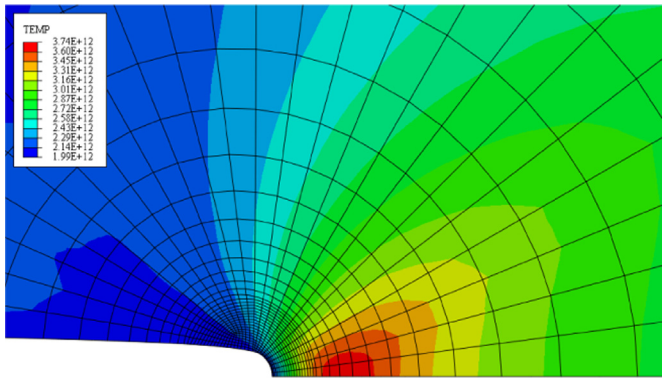

Fig. 3. Hydrogen lattice concentration at 130 s.

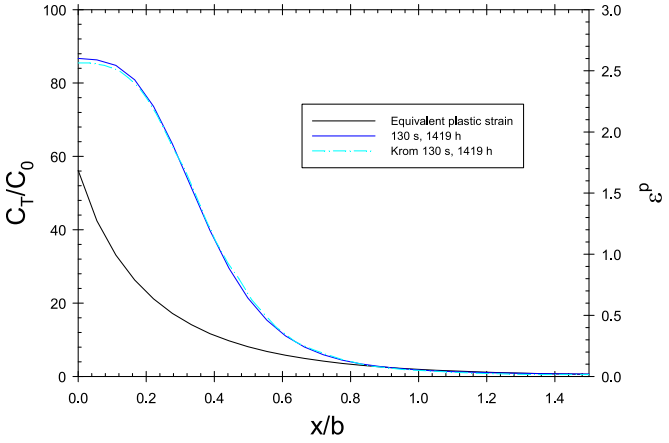

Fig. 5. Hydrogen concentration in trapping sites. Comparison with Ref. [2] (dashed lines).

4.3.3. Results

Hydrogen lattice distribution follows that of the hydrostatic stress, as expected, reaching the peak concentration at approximately 0.07 mm from the crack tip (Fig. 3).

Plotting concentration profiles (Fig. 4) with and without plastic strain rate (last term in Eq. (20)), along the x axis (normalized by the crack tip opening displacement b) in the crack plane, results perfectly fit those of Krom et al. [2]. Small differences in crack tip are due to refining the mesh.Therefore, UMATHT subroutine is regarded as a valid method for simulating hydrogen transport near a crack tip. As Krom et al. [2] demonstrated, considering plastic strain rate $\partial\varepsilon^p/\partial t$ results in a greater concentration C_L at 130 s while it does not alter distribution at 1419 h.

Once C_L is known, hydrogen concentration in traps C_T is obtained through Eq. (17). At the crack tip (x=0), trapped hydrogen is about 86 times greater than C_{eq} (Fig. 5) so it has a much greater weight in the total concentration ($C = C_L+C_T \approx C_T$). This is due to the large plastic deformation levels in the crack tip. Contrasting with interstitial hydrogen, hydrogen distribution in traps at 130 s nearly corresponds with that of the steady state at 1419 h. It has to be noted that the plotted x/b range is greater in Fig. 4 (0.0–5.0) than in Fig. 5 (0.0–1.5) so direct visual comparison can be misleading.

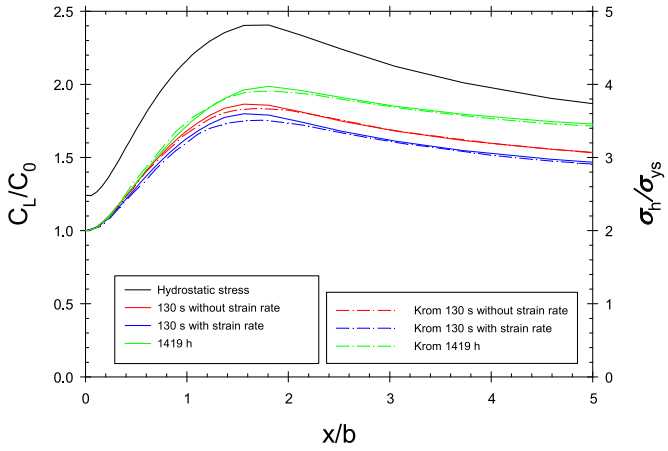

Fig. 4. Hydrogen lattice concentration with and without plastic strain rate. Comparison with Ref. [2] (dashed lines).

4.4. Simulation of coupled effects

Geometry, diffusion parameters and loads are the same that those of the previous section. Only coupling Eqs. (26) and (27) modify the transport model.

4.4.1. Coupling parameters

With the meaning above mentioned in Eq. (24), volume change for each introduced atom Δv is related to the partial molar volume: $\Delta v = \bar{V}_H/N_A$, being N_A Avogadro's number.

The mean volume of an iron atom Ω is the inverse of the iron atom concentration N_{Fe} Eq. (38).

Hydrogen concentrations, c and c_0, are expressed in total H atoms per metal atom; consequently, they must be expressed in terms of lattice and trap concentration in order to couple the transport equations:

$$c = \frac{C_L + C_T}{N_{Fe}} \tag{41}$$

Additionally, initial concentration in the unstressed state is taken as the equilibrium concentration per metal atom: $c_0 = C_{eq}/N_{Fe}$ (Table 3).

Local softening parameter ξ is difficult to interpret because it does not have physical meaning. From Kotake et al. [14], $1+\xi$

Table 3
Coupling parameters.

Δv	$3.3211\cdot10^{-21}$ mm^3/atH
Ω	$1.1764\cdot10^{-20}$ mm^3/atFe
λ	0.2826
c_0	$2.4469\cdot10^{-8}$ atH/atFe
ξ	$-2.0434\cdot10^{6}$ / 0 / $+2.0434\cdot10^{6}$

factor can be seen as how much the yield stress increases (or decreases if $\xi<0$) when the normalized concentration has reached its maximum, i.e. $c=1$. However, this maximum concentration is difficult to reproduce experimentally so in this work the equilibrium concentration is the reference value. For example, it is supposed that at C_{eq} yield stress has been reduced by 5%. Then:

$$\xi c_0 + 1 = 0.95 \tag{42}$$

Thus with $c_0=2.4469\cdot10^{-8}$ atH/atFe, coupling parameter is $\xi=-2.0434\cdot10^{6}$.

Three scenarios are simulated:

- Hydrogen does not affect plastic flow, thus $\xi=0$ and only dilatation is considered.
- At equilibrium concentration, $C_{eq}=2.08\cdot10^{12}$ H atoms/mm^3, yield stress is reduced by 5%, corresponding to $\xi=-2.0434\cdot10^{6}$ which indicates local softening.
- At equilibrium concentration, $C_{eq}=2.08\cdot10^{12}$ H atoms/mm^3, yield stress is increased by 5%, corresponding to $\xi=+2.0434\cdot10^{6}$ which indicates local hardening.

4.4.2. Results

4.4.2.1. Dilatation. Following the boundary layer approach, the work of Taha and Sofronis [21], usually cited in hydrogen diffusion modelling papers, is taken for the sake of comparison.

However, only dilatation is considered by these authors, i.e. $\xi=0$. Therefore, simulation with $\xi=0$ and $\lambda=0.2816$ has been performed and hydrogen concentration in lattice sites is plotted (solid line with white triangles in Fig. 6) and compared with [21] (green dashed line in Fig. 6). Results agree well and small deviation is attributed to numerical implementation and meshing differences.

Results also show that dilatation does not modify hydrogen concentration distribution as results considering $\lambda=0.2816$ coincide with $\lambda=0$, i.e. hydrogen induced dilatation strain does not affect hydrogen transport. This was expected because hydrogen has a low solubility in iron so parameters λ and c_0 are too low. In the case of high solubility systems (e.g. Niobium), as demonstrated by Lufrano et al. [4], dilatation significantly alter hydrogen transport.

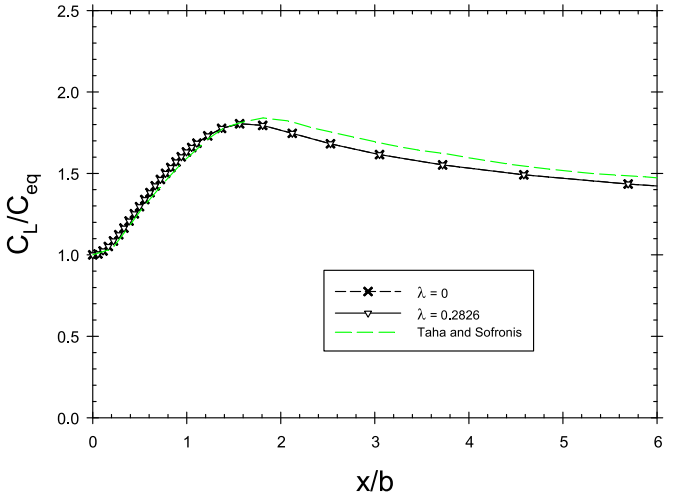

Fig. 6. Hydrogen lattice concentration at 130 s with and without dilatation parameter λ. Comparison with Ref. [21] (green dashed lines). Results include equilibrium concentration C_{eq} range from $2.08\cdot10^{12}$ to $1\cdot10^{20}$ atH/mm^3. (For interpretation of the references to color in this figure legend, the reader is referred to the web version of this article.)

Keeping $\lambda=0.2816$, higher equilibrium concentrations C_{eq} have been simulated, leading to higher c_0 parameters; there are not changes in C_L distributions in any case (solid line with white triangles in Fig. 6). This means that even under extreme conditions (very high H_2 fugacity in gaseous charging [22] or high overpotential in electrochemical charging [23]) hydrogen dilatation may be neglected in transport simulations.

However, it has been taken into account that for high equilibrium concentrations, lattice occupancy approximates to one: $\theta_L\approx1$, i.e. $C_{eq}=N_L$, so simplifications made in Section 2.3. are not consistent and results might not be accurate; in any case, these extreme high values of lattice occupancy are nearly impossible to find experimentally in steel due to its low solubility, so it is presumed that dilatation can be always neglected.

4.4.2.2. Hardening/Softening. Considering plastic flow modified by hydrogen concentration, lattice hydrogen concentrations are plotted (Fig. 7). Enhanced softening ($\xi=-2.04\cdot10^{6}$) results in a minor hydrostatic stress distribution and thus a smaller hydrogen lattice concentration.

Results are qualitatively discussed because they lack empirical base. Hardening or softening parameter ξ should be experimentally fitted. Atomistic simulations of dislocation interactions with hydrogen could also lead to a better understanding of this microscale phenomenon.

5. Flux between traps

One of the simplifications assumed was that $J_T=0$. In a crack tip, it is arguably whether traps are isolated amongst each other or not, so simulation with all of the parameters used in Section 4.2 is performed again, but this time considering flux between traps different from zero, according to Eq. (10). It is important to note that in the gradient of the number of trapping sites, a plastic strain gradient appears. For example, if the Kumnick and Johnson expression (21) is considered:

$$\nabla N_T = 29.50762797\cdot N_T\cdot\nabla\varepsilon_p\cdot\exp\left(-5.5\cdot\varepsilon_p\right) \tag{43}$$

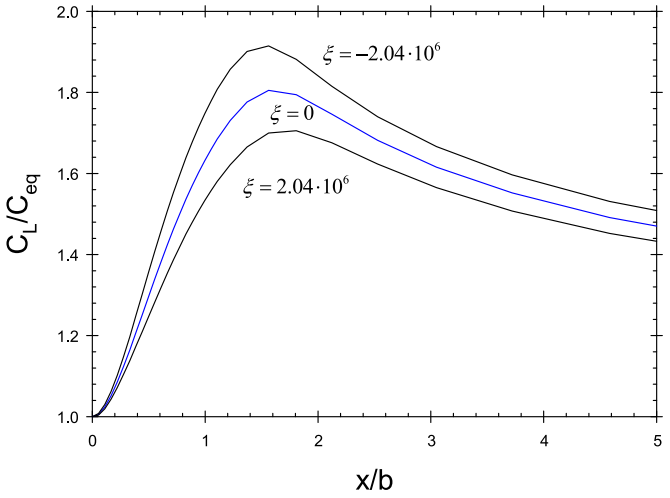

Fig. 7. Hydrogen lattice concentration with softening ($\xi=-2.04\cdot10^{6}$) and hardening ($\xi=2.04\cdot10^{6}$) effects.

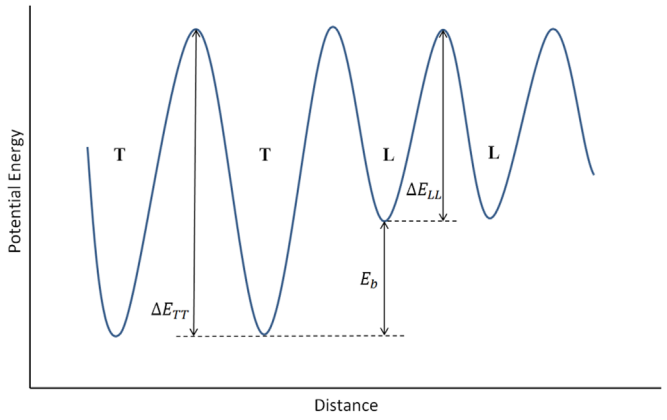

Fig. 8. Potential energy trace and energetic relationships between trapping sites (T) and lattice sites (L).

In the present paper, classical theory of plasticity is assumed, however, considering plastic strain gradients could lead to implementing the gradient-enhanced local hardening predicted by Strain Gradient Plasticity (SGP) [24,25]. Moreover, the role played by Geometrically Necessary Dislocations (GND) associated with these gradient theories in hydrogen trapping is still not well understood. Taking into account SGP in hydrogen diffusion near a crack tip [26] could represent a breakthrough for Hydrogen Assisted Cracking modelling [27].

To account for J_T, diffusivity between trapping sites must be included. Diffusion coefficient between two different sites, *i* and *j*, has the following expression:

$$D_{ij} = \omega_{0i} \cdot l_{ij}^2 \cdot \exp\left(-\frac{\Delta E_{ij}}{RT}\right) \tag{44}$$

Assuming the same pre-exponential factor, i.e. the same frequency of vibration and the same hopping length, an energetic relation might be established: $\Delta E_{TT} - \Delta E_{LL} = E_b$ (Fig. 8). Saddle points in the potential energy distribution are supposed constant.

From Eq. (44), the inherently negative binding energy E_b defines the equilibrium constant K_T as in Eq. (16). Diffusivities might be related as follows:

$$D_{TT} = \frac{D_{LL}}{K_T} \tag{45}$$

With the binding energy $E_b = -60$ kJ/mol and D_{LL}=0.0127 mm^2/s, chosen from Ref. [1], D_{TT}=4.53·10^{-13} mm^2/s. Results in Fig. 9 compare simulation without considering J_T (from Fig. 4 at 130 s) with indicate that flux between trapping sites can be neglected so the simplification made before is valid. However, this validity has to be connected to specific parameters, in this case with a high binding energy and its consequent very low D_{TT}.

If the simulation is repeated only decreasing the absolute value of the binding energy from −60 kJ/mol to −10 kJ/mol, the diffusivity D_{TT} increases exponentially (D_{TT}=2.30·10^{-4} mm^2/s), but as Oriani's equilibrium has been supposed, hydrogen concentration in trapping sites is nearly zero C_T (Fig. 10). Therefore, results of concentration change respect Section 4.2 but flux between traps might be neglected again.

It must be concluded that, even though binding energy is an influential parameter, remoteness of trapping sites between them is the crucial factor when considering flux J_T [9]. In order to assume that traps are not connected, the ratio between N_T and N_L must be considered. If the number of traps is high compared with the number of interstices, the crystal has many defects and J_T cannot be neglected; this approach could explain the accelerated

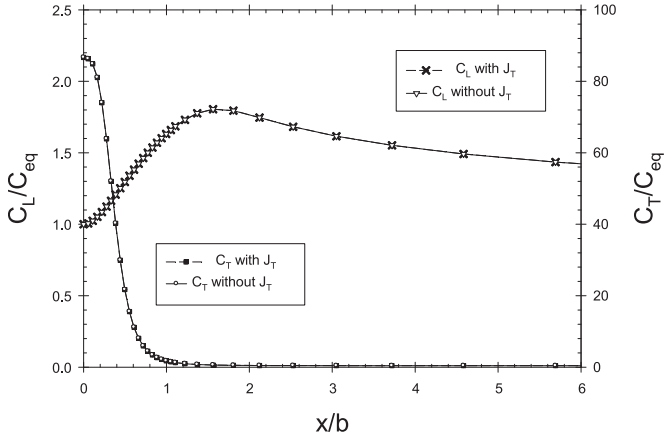

Fig. 9. Hydrogen concentration at 130 s in trapping sites (C_T) and lattice sites (C_L) with and without considering flux between traps J_L with binding energy E_b = −60 kJ/mol.

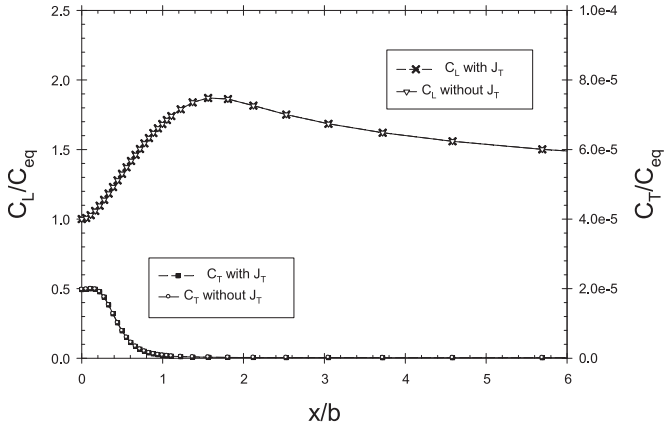

Fig. 10. Hydrogen concentration at 130 s in trapping sites (C_T) and lattice sites (C_L) with and without considering flux between traps J_L with binding energy E_b = −10 kJ/mol.

diffusion or "pipe diffusion" found in grain boundaries [28] or dislocation cores [29].

Toribio and Kharin [9] discuss the generalized model and the particular simplifications from discrete random walking principles. Therefore fluxes include explicitly the jump success probability from two different places. However, comparison with phenomenological models based on Onsager's approach present several difficulties. For instance, parameters L_{ij} can be related to diffusivites D_{ij}, as made in Eqs. (5) and (6), from atomistic arguments in solid solutions [30]. More effort to bridge both approaches must be made.

6. Boundary conditions

Previously only simulations with a constant hydrogen concentration C_{eq} in the crack tip have been shown. Referenced works [1,2,5,21] also include an insulated situation, equivalent to a zero flux perpendicular to the boundary (*zero flux boundary condition*). Different expressions of hydrogen flux as a boundary condition have been discussed, especially when hydrogen is inserted electrochemically [17,23,27] with a particular application for permeation modelling. Turnbull [27] underlines that the entering flux depends also on hydrostatic stress. In the case of hydrogen concentration as a boundary condition, this also can be shown. Assuming a balance between the diatomic hydrogen gas at the surface and the hydrogen atom in solution inside the metal [22]:

$$\frac{1}{2}H_2 \leftrightarrow H \tag{46}$$

From this equilibrium, the following relation between chemical potential must be met:

$$\frac{1}{2}\mu_{H_2} = \mu_H \tag{47}$$

Where chemical potential of hydrogenous gas μ_{H_2} depends on its chemical activity or its fugacity f_{H_2} [5]:

$$\mu_{H_2} = \mu_{H_2}^0 + RT \ \ln\left(\frac{f_{H_2}}{p^0}\right) \tag{48}$$

Chemical potential of hydrogenous gas in the standard state (p^0=1 atm and T=25°C) is zero: $\mu_{H_2}^0$=0; therefore p^0 might be omitted provided fugacity is expressed in atmospheres. Electrolytic charging of hydrogen is equivalent to gaseous charging if both methods produce the same fugacity; in electrolytic charging fugacity depends on overpotential [23] while in gaseous charging fugacity depends on pressure [22].

Substituting (48) in Eq. (47), it can be concluded that chemical potential of hydrogen in solution in the boundary follows the expression:

$$\mu_H = RT \ \ln\left(\sqrt{\frac{f_{H_2}}{p^0}}\right) \tag{49}$$

It is supposed that this hydrogen atom is placed in a lattice site, i.e. μ_H=μ_L; thus with Eq. (7), and assuming again low occupancy, $\theta_L \ll 1$, a boundary concentration is obtained:

$$C_L = \frac{N_L}{\sqrt{p^0}} \exp\left(-\frac{\mu_L^0}{RT}\right)\exp\left(\frac{\bar{V}_H \sigma_h}{RT}\right)\sqrt{f_{H_2}} \tag{50}$$

This expression might be grouped in the Sievert's law form, with solubility K and fugacity instead of pressure:

$$C_L = K\sqrt{f_{H_2}} \tag{51}$$

Terms included in solubility demonstrate that it follows an Arrhenius law and it should be expressed in units of concentration divided by pressure (e.g. atH·m^{-3}·MPa$^{-1/2}$). It is also crucial to note that apparent solubility increases with hydrostatic stress due to the lower chemical potential in regions under tension. If equivalent concentration C_{eq} included in the previous simulations is only considered in the unstressed state (with solubility $K_{\sigma_h=0}$), then the realistic boundary condition should be:

$$C_L = C_{eq} \ \exp\left(\frac{\bar{V}_H \sigma_h}{RT}\right) \tag{52}$$

Di Leo and Anand [5] realised that analytic solution of diffusion in steady state, i.e. when fluxes definitely become zero, follows this expression but simulations made by several authors (e.g. Sofronis and McMeeking [1], Krom et al. [2], etc.) did not. The reason is because stress state must be included in the boundary condition. Di Leo and Anand consider hydrogen chemical potential as the finite element unknown variable, instead of hydrogen lattice concentration, so Eq. (52) is their boundary condition.

In this paper two approaches are merged: the implementation of appropriate boundary conditions according to Eq. (52), and the use of the heat transfer analogy described in previous sections. To this end, in addition to the previously mentioned subroutines, a DISP subroutine is used, allowing one to enter a user-defined boundary condition. DISP works with nodal values while the hydrostatic stress is calculated at the integration points, so an interpolation should be performed by means of the shape functions.

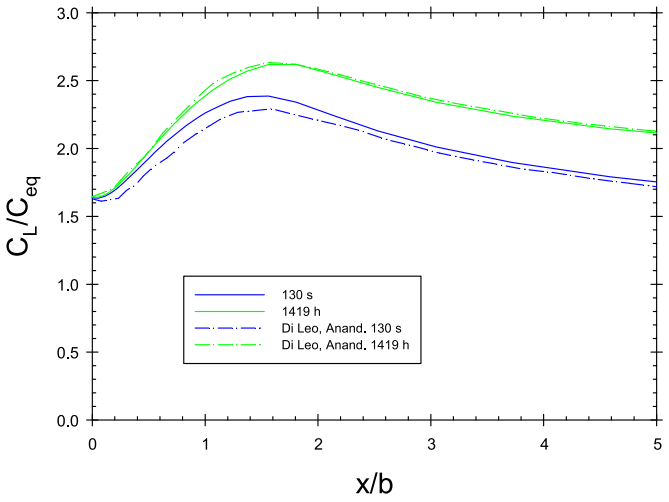

Fig. 11. Hydrogen lattice concentration with stress-dependent boundary condition. Comparison with Ref. [5].

Hydrogen diffusion near a crack tip is simulated again without coupling effects and with the parameters of Table 2 but now with the stress-dependant boundary concentration.

Results (Fig. 11) agree perfectly for 1419 h and with a slight deviation for 130 s with those obtained by Di Leo and Anand. The most remarkably conclusion is that there is a considerable increase in hydrogen lattice concentration compared to simulations that do not consider stress state in the boundary conditions. Moreover, hydrogen distribution at 1419 h perfectly matches with analytical solution of the steady state.

7. Conclusions

Simulations of hydrogen transport in a crack tip must include the hydrostatic stress as a driving variable, since it modifies the chemical potential. Moreover, the level of plastic strain is always associated with an increase in the number of traps, causing the creation of defects in the form of dislocations. Including σ_h and ε^p as variables within the diffusion equations, the stress-strain field in the crack tip predicts peak hydrogen concentrations.

The same results as Refs. [1,2,5,21] were obtained in crack tip through the boundary layer approach. Interstitial hydrogen concentration has a peak, about 1.5 to 2 times the boundary concentration, due to the hydrostatic stress peak at a certain distance from the crack tip. However, consideration of traps associated with plastic strain causes hydrogen concentration in trapping sites to show a maximum of approximately 80 times C_{eq} just at the crack tip. The location of critical hydrogen concentration is crucial in order to pinpoint the Fracture Process Zone.

In addition, implementation of the plastic strain rate term in UMATHT subroutine confirms the results of Krom et al. [2]: the velocity at which traps are created influences the concentration for short times, but it does not alter the hydrogen distribution in the steady state. When loading rates are very high, thermodynamic equilibrium proposed by Oriani might not be fulfilled, and thus a kinetic formulation for the exchange between traps and lattice sites must be used.

This paper makes use of the expression from Kumnick and Johnson [12] that relates the number of traps with plastic strain. However, the concept of trap comprises many defect types in a metal lattice (e.g. grain boundaries, inclusions, vacancies, etc.) that are not a direct consequence of plastic deformation. In addition, each trap has a different associated binding energy. Both the concentration of each type of trap within the bulk material and its

corresponding energy characteristics should be better studied at some point in the future.

Flux between traps is neglected, as in the revisited literature, and this assumption is verified numerically, as it has been confirmed that for the parameters used by Sofronis and McMeeking for alpha iron [1], J_T is insignificant. For traps with high binding energy, diffusivity between trapping sites always has a very low value (irreversible traps), while for traps with low binding energy, Oriani's balance predicts very low concentrations in trapping sites; in both cases J_T is nearly zero. However, the concept of proximity or remoteness should be explicitly included when discussing whether flux between traps occurs or not.

It is also essential to know how the hydrogen concentration influences the elasto-plastic material response, i.e. the so-called coupled diffusion. By means of subroutines that continue with the heat transfer analogy (UEXPAN and UHARD), coupled diffusion has been implemented more easily without directly rewriting the material constitutive equations and its tangent stiffness. It has been concluded that dilation in alpha iron is negligible even for very high concentrations which only occur under extreme conditions. Nevertheless, for other metals and lattice arrangements, dilatation modelling might be unavoidable, especially in those metals that form hydrides.

Hydrogen influence on plastic flow cannot be easily modelled, since each particular situation may lead to either a local softening or a local hardening. The coupling parameter ξ would be best interpreted from a microstructural point of view; to this end, interaction of hydrogen with dislocations should be better understood.

Besides the coupling of diffusion, boundary conditions are crucial in simulation results. However, they have been usually overlooked, and little attention is paid to its stress state dependence. In this paper, from the expression of a chemical potential constant at the boundary, a hydrogen concentration dependent on hydrostatic stress has been implemented as a boundary condition. In future research, the hydrogen entry is to be modelled more realistically, considering both gaseous and electrochemical conditions.

The analogy between heat transfer and hydrogen diffusion is not only useful for transport modelling; ABAQUS allows the inclusion of temperature-dependencies in laws of damage, e.g. Traction Separation Law in the Cohesive Zone Model, and therefore the inclusion of dependencies on the analogous hydrogen concentration.

As an important disadvantage, the present heat transfer subroutines are only valid for isothermal models. Efforts must be made in order to implement Finite Element models considering thermophoresis, i.e. how temperature gradients affect hydrogen diffusion.

Acknowledgments

The authors are grateful for the funding received from project MINECO Ref: MAT2014-58738-C3-2-R and from the grant JCYL EDU/1006/2015. E. Martinez-Pañeda is also acknowledged for helpful discussions.

References

[1] Sofronis P, McMeeking RM. Numerical analysis of hydrogen transport near a blunting crack tip. J Mech Phys Solids 1989;37:317–50.
[2] Krom A, Koers R, Bakker A. Hydrogen transport near a blunting crack tip. J Mech Phys Solids 1999;47:971–92.
[3] Sofronis P, Liang Y, Aravas N. Hydrogen induced shear localization of the plastic flow in metals and alloys. Eur J Mech - A/Solids 2001;20:857–72.
[4] Lufrano J, Sofronis P, Birnbaum HK. Elastoplastically accommodated hydride formation and embrittlement. J Mech Phys Solids 1998;46:1497–520.
[5] Di Leo CV, Anand L. Hydrogen in metals: a coupled theory for species diffusion and large elastic–plastic deformations. Int J Plast 2013;43:42–69.
[6] Díaz A, Alegre JM, Cuesta II. A review on diffusion modelling in hydrogen related failures of metals. Eng Fail Anal 66, 2016, 577–595.
[7] Onsager L. Reciprocal relations in irreversible processes. I. Phys Rev 1931;37:405.
[8] Onsager L. Reciprocal relations in irreversible processes. II. Phys Rev 1931;38:2265.
[9] Toribio J, Kharin V. A generalised model of hydrogen diffusion in metals with multiple trap types. Philos Mag 2015:1–23.
[10] Oriani RA. The diffusion and trapping of hydrogen in steel. Acta Metall 1970;18:147–57.
[11] McNabb A, Foster PK. A new analysis of the diffusion of hydrogen in iron and ferritic steels. Trans Metall Soc AIME 1963;227:618–27.
[12] Kumnick AJ, Johnson HH. Deep trapping states for hydrogen in deformed iron. Acta Metall 1980;28:33–9.
[13] Birnbaum HK, Sofronis P. Hydrogen-enhanced localized plasticity—a mechanism for hydrogen-related fracture. Mater Sci Eng: A 1994;176:191–202.
[14] Kotake H, Matsumoto R, Taketomi S, Miyazaki N. Transient hydrogen diffusion analyses coupled with crack-tip plasticity under cyclic loading. Int J Press Vessel Pip 2008;85:540–9.
[15] Oh C-S, Kim Y-J, Yoon K-B. Coupled analysis of hydrogen transport using ABAQUS. J Solid Mech Mater Eng 2010;4:908–17.
[16] Kim N-H, Oh C-S, Kim Y-J, Yoon K-B, Ma Y-W. Hydrogen-assisted stress corrosion cracking simulation using the stress-modified fracture strain model. J Mech Sci Technol 2012;26:2631–8.
[17] Falkenberg R, Brocks W, Dietzel W, Scheider I. Modelling the effect of hydrogen on ductile tearing resistance of steels: dedicated to Professor Dr. Hermann Riedel on the occasion of his 65th birthday. Int J Mater Res 2010;101:989–96.
[18] Bird RB, Stewart WE, Lightfoot EN. Transport phenomena. New York: John Wiley & Sons; 2007.
[19] Barrera O, Tarleton E, Tang HW, Cocks ACF. Modelling the coupling between hydrogen diffusion and the mechanical behaviour of metals. Comput Mater Sci 2016;122:219–28.
[20] Miresmaeili R, Ogino M, Nakagawa T, Kanayama H. A coupled elastoplastic-transient hydrogen diffusion analysis to simulate the onset of necking in tension by using the finite element method. Int J Hydrog Energy 2010;35:1506–14.
[21] Taha A, Sofronis P. A micromechanics approach to the study of hydrogen transport and embrittlement. Eng Fract Mech 2001;68:803–37.
[22] Marchi CS, Somerday BP, Robinson SL. Permeability, solubility and diffusivity of hydrogen isotopes in stainless steels at high gas pressures. Int J Hydrog Energy 2007;32:100–16.
[23] Liu Q, Atrens AD, Shi Z, Verbeken K, Atrens A. Determination of the hydrogen fugacity during electrolytic charging of steel. Corros Sci 2014;87:239–58.
[24] Hutchinson JW. Plasticity at the micron scale. Int J Solids Struct 2000;37:225–38.
[25] Fleck NA, Hutchinson JW. A phenomenological theory for strain gradient effects in plasticity. J Mech Phys Solids 1993;41:1825–57.
[26] Martínez-Pañeda E, del Busto S, Niordson CF, Betegón C. Strain gradient plasticity modeling of hydrogen diffusion to the crack tip. Int J Hydrog Energy.
[27] Turnbull A. Perspectives on hydrogen uptake, diffusion and trapping. Int J Hydrog Energy 40, 2015, 16961–16970.
[28] Oudriss A, Creus J, Bouhattate J, Conforto E, Berziou C, Savall C, Feaugas X. Grain size and grain-boundary effects on diffusion and trapping of hydrogen in pure nickel. Acta Mater 2012;60:6814–28.
[29] Zhang X, Peng Q, Lu G. Self-consistent embedding quantum mechanics/molecular mechanics method with applications to metals. Phys Rev B 2010;82:134120.
[30] Choudhury S, Barnard L, Tucker JD, Allen TR, Wirth BD, Asta M, Morgan D. Ab-initio based modeling of diffusion in dilute bcc Fe–Ni and Fe–Cr alloys and implications for radiation induced segregation. J Nucl Mater 2011;411:1–14.